SCIENCE CHINA
Physics, Mechanics & Astronomy

• Article •

June 2024 Vol. 67 No. 6: 260312
https://doi.org/10.1007/s11433-023-2340-7

Quantum squeezing induced nonreciprocal phonon laser

Tian-Xiang Lu[1,2], Yan Wang[3], Keyu Xia[4], Xing Xiao[1], Le-Man Kuang[2,3], and Hui Jing[2,3*]

[1] *College of Physics and Electronic Information, Gannan Normal University, Ganzhou 341000, China;*
[2] *Key Laboratory of Low-Dimensional Quantum Structures and Quantum Control of Ministry of Education, Department of Physics and Synergetic Innovation Center for Quantum Effects and Applications, Hunan Normal University, Changsha 410081, China;*
[3] *Academy for Quantum Science and Technology, Zhengzhou University of Light Industry, Zhengzhou 450002, China;*
[4] *College of Engineering and Applied Sciences, National Laboratory of Solid State Microstructures, and Collaborative Innovation Center of Advanced Microstructures, Nanjing University, Nanjing 210023, China*

Received December 3, 2023; accepted February 2, 2024; published online May 14, 2024

Phonon lasers or coherent amplifications of mechanical oscillations are powerful tools for fundamental studies on coherent acoustics and hold potential for diverse applications, ranging from ultrasensitive force sensing to phononic information processing. Here, we propose the use of an optomechanical resonator coupled to a nonlinear optical resonator for directional phonon lasing. We find that by pumping the nonlinear optical resonator, directional optical squeezing can occur along the pump direction. As a result, we can achieve the directional mechanical gain using directional optical squeezing, thereby leading to nonreciprocal phonon lasing with a well-tunable directional power threshold. Our work proposes a feasible way to build nonreciprocal phonon lasers with various nonlinear optical media, which are important for a wide range of applications, such as directional acoustic amplifiers, invisible sound sensing or imaging, and one-way phononic networks.

nonreciprocal phonon laser, directional quantum squeezing, optomechanics

PACS number(s): 71.36.+c, 42.65.Yj, 42.50.-p

Citation: T.-X. Lu, Y. Wang, K. Xia, X. Xiao, L.-M. Kuang, and H. Jing, Quantum squeezing induced nonreciprocal phonon laser, Sci. China-Phys. Mech. Astron. **67**, 260312 (2024), https://doi.org/10.1007/s11433-023-2340-7

1 Introduction

Phonon lasers or coherent amplifications of mechanical oscillations have played an essential role in fundamental studies on coherent acoustics and show potential in applications ranging from sound imaging or sensing [1-5] to topological motion control [6] and phononic engineering [7, 8]. In recent years, phonon lasers have been experimentally achieved in diverse platforms: as trapped ions [9, 10], cold atoms [11], optical tweezers [12, 13], and cavity optomechanical (COM) systems [14-19], to name a few [20-25]. In particular, COM devices [26], which are suitable for integration into chip scales, have been used to realize different phonon laser types [27-35], such as exceptional-point [27-29], phase-modulated [30, 31], and vector [32, 33] phonon lasers.

Recently, nonreciprocal phononic devices, featuring directional phonon flow, were explored and utilized for chiral phonon transport or cooling [36-38], phonon isolation [39-44], one-way mechanical networks [45-51], and backscattering-immune acoustic sensing or imaging [52, 53]. In these studies, nonreciprocal acoustic or optical control has been achieved by incorporating nonlinear media [40-45], circulating fluids [39], macroscopic metamaterials [46-49],

*Corresponding author (email: jinghui73@gmail.com)

space-time modulation [54, 55], optomechanical interaction [56-62], and complex synthetic structures [51]. In particular, nonreciprocal phonon lasers were proposed using the relativistic Sagnac effect in a spinning COM device or magnomechanical system [63, 64], enabling the highly asymmetric operation of phonon lasers. However, in these studies [63, 64], high-speed rotation of resonators is required; hence, they need to strongly rely on stable couplings between spinning devices and flying fibers. Therefore, a new approach that is free of any spinning component and is easily tunable optically is highly desired.

In a very recent study, directional quantum squeezing was proposed to achieve an optical diode or circulator [65], opening up an attractive route for preparing nonreciprocal devices via harnessing various quantum resources. We note that the advantages of quantum squeezing, e.g., a considerable amplification of light-motion interactions or coherent coupling of hybrid quantum systems, have also been confirmed [66-85]. Based on one-way squeezing, nonreciprocal photonic or magnonic devices have also been explored [86-89]. Inspired by these pioneering works, here, we study the use of directional optical squeezing to achieve a nonreciprocal phonon laser in a compound COM system. We find that asymmetric coupling of resonators can be achieved by unidirectionally driving the nonlinear optical resonator, resulting in nonreciprocal mechanical gains and a well-tunable direction-dependent threshold of phonon lasing. Furthermore, we find that in such nonreciprocal devices, the mechanical gain exhibits squeezing-enhanced robustness against optical decays. Our scheme, requiring only two-mode optical frequency matching and free of any spinning device, has potential to be realized under current experimental conditions and thus can be utilized for applications such as nonreciprocal force sensing and chiral acoustic information processing or networking [36, 37].

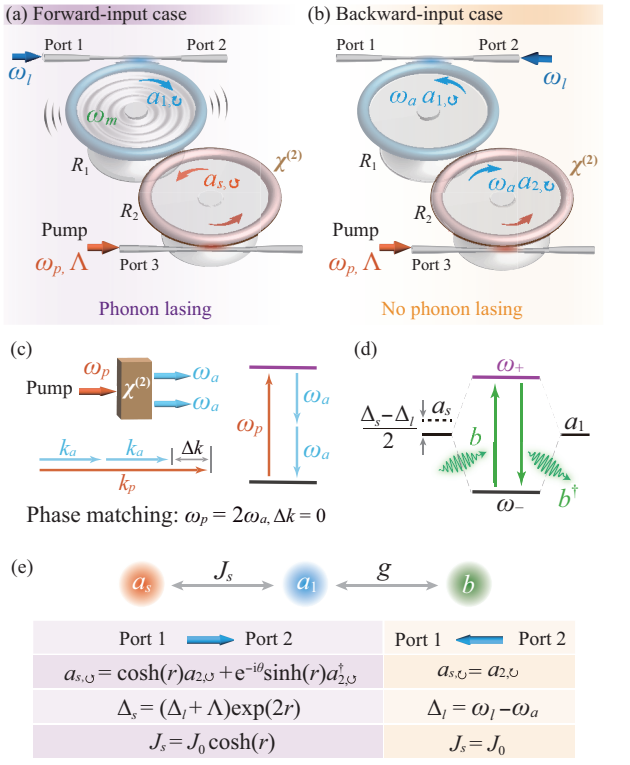

Figure 1 (Color online) Operating a nonreciprocal phonon laser with directional squeezing. A strong pump with frequency ω_p and strength Λ, coming from port 3, causes the counterclockwise (CCW) mode to be squeezed, i.e., $a_{2,\circlearrowleft} \to a_{s,\circlearrowleft}$, in the nonlinear optical resonator R_2. (a) The input laser with frequency ω_l driven by port 1 excites the clockwise mode $a_{1,\circlearrowright}$ in R_1, which is coupled to a squeezed mode $a_{s,\circlearrowleft}$ in R_2 with effective strength J_s; meanwhile, in (b), when driven from port 2, the input laser excites the CCW mode $a_{1,\circlearrowleft}$ in R_1, which is coupled to a unsqueezed mode $a_{2,\circlearrowleft}$ in R_2 with strength J_0. (c) The nonlinear parametric process: a pump photon with frequency ω_p and wavenumber k_p can be down-converted into two photons with the same frequency ω_a and wavenumber k_a due to the $\chi^{(2)}$ nonlinearity under the phase-matching condition. (d) The energy-level diagram shows the mechanism of a two-level phonon laser, i.e., stimulated phonon emissions under the population inversion condition (for the optical supermodes $\omega_\pm$). (e) Comparison of direction-dependent key symbols in forward-input and backward-input cases. Here, r is the squeezing parameter.

2 Theoretical model

As shown in Figure 1, we consider a compound COM system comprising two coupled whispering-gallery-mode (WGM) microtoroid resonators and two nearby optical waveguides. The resonator R_1 with resonance frequency ω_a and decay rate κ_1 supports a mechanical breathing mode (with frequency ω_m and effective mass m) and is driven by a driving field of frequency ω_l from port 1 (or port 2) corresponding to the forward-input case (or backward-input case). The other resonator R_2 with resonance frequency ω_a and decay rate κ_2 is manufactured using high-quality thin film with $\chi^{(2)}$ nonlinearity [90-101]. Thus, the resonator supports the parametric amplification process [66] and is pumped from port 3 via a continuous coherent laser field with frequency ω_p, strength Λ, and phase θ.

As shown in Figure 1(c), because of the directional phase-matching condition in the parametric nonlinear process [65, 98], i.e., the conservation of energy and momentum ($\omega_p = 2\omega_a$, $\Delta k = 0$), the counterclockwise (CCW) mode $a_{2,\circlearrowleft}$ is squeezed to a mode $a_{s,\circlearrowleft}$, while the clockwise (CW) mode $a_{2,\circlearrowright}$ is unsqueezed [65, 86, 87, 89]. For the forward-input case, in a frame rotating at frequency ω_l, the total Hamiltonian of this system can be written at the simplest level as follows:

$$\begin{aligned}\mathcal{H} =& -\Delta_l a^\dagger_{1,\circlearrowleft}a_{1,\circlearrowleft} - \Delta_l a^\dagger_{2,\circlearrowleft}a_{2,\circlearrowleft} + \omega_m b^\dagger b \\ &+ J_0(a^\dagger_{1,\circlearrowleft}a_{2,\circlearrowleft} + a^\dagger_{2,\circlearrowleft}a_{1,\circlearrowleft}) - g x_0 a^\dagger_{1,\circlearrowleft}a_{1,\circlearrowleft}(b + b^\dagger)\end{aligned}$$

$$+ \mathrm{i}\varepsilon_l(a^\dagger_{1,\circlearrowleft} - a_{1,\circlearrowleft}) + \frac{\Lambda}{2}(a^{\dagger 2}_{2,\circlearrowleft}\mathrm{e}^{-\mathrm{i}\theta} + a^2_{2,\circlearrowleft}\mathrm{e}^{\mathrm{i}\theta}), \quad (1)$$

where $a_{1,\circlearrowleft}$ ($a^\dagger_{1,\circlearrowleft}$), $a_{2,\circlearrowleft}$ ($a^\dagger_{2,\circlearrowleft}$), and b ($b^\dagger$) are the annihilation (creation) operators of the CW mode in R_1, CCW mode in R_2, and mechanical mode in R_1, respectively. $\Delta_l = \omega_l - \omega_a$, J_0 (or $g = \omega_a/r_1$) denotes the coupling strength between resonators (or the COM coupling strength), $x_0 = \sqrt{\hbar/2m\omega_m}$, and r_1 is the radius of the COM resonator. $\varepsilon_l = \sqrt{2\kappa_1 P_{\mathrm{in}}/\hbar\omega_l}$ is the driving strength with input power P_{in}. To diagonalize $\mathcal{H}$, we define the squeezed operator $a_{s,\circlearrowleft}$ via the Bogoliubov transformation [66, 68], as follows:

$$a_{s,\circlearrowleft} = \cosh(r)a_{2,\circlearrowleft} + \mathrm{e}^{-\mathrm{i}\theta}\sinh(r)a^\dagger_{2,\circlearrowleft}, \quad (2)$$

with the squeezing parameter $r = (1/4)\ln[(\Delta_l - \Lambda)/(\Delta_l + \Lambda)]$, which requires $|\Delta_l| > |\Lambda|$ to avoid system instability. Subsequently, applying the rotating-wave approximation (refer to Appendix for more details), the Hamiltonian of the system becomes

$$\begin{aligned}\mathcal{H}_{\mathrm{f}} =& -\Delta_l a^\dagger_{1,\circlearrowleft}a_{1,\circlearrowleft} - \Delta_s a^\dagger_{s,\circlearrowleft}a_{s,\circlearrowleft} + J_s(a^\dagger_{1,\circlearrowleft}a_{s,\circlearrowleft} + a^\dagger_{s,\circlearrowleft}a_{1,\circlearrowleft})\\ &+ \omega_m b^\dagger b - g x_0 a^\dagger_{1,\circlearrowleft}a_{1,\circlearrowleft}(b + b^\dagger) + \mathrm{i}\varepsilon_l(a^\dagger_{1,\circlearrowleft} - a_{1,\circlearrowleft}), \quad (3)\end{aligned}$$

where

$$\Delta_s = (\Delta_l + \Lambda)\exp(2r), \quad J_s = J_0\cosh(r). \quad (4)$$

The effective squeezed mode detuning Δ_s and effective coupling rate J_s are modulated by the squeezing strength Λ under the condition of ensuring system stability (e.g., $|\Delta_l| > |\Lambda|$). For the backward-input case, the Hamiltonian of the system can be written as follows:

$$\begin{aligned}\mathcal{H}_{\mathrm{b}} =& -\Delta_l a^\dagger_{1,\circlearrowleft}a_{1,\circlearrowleft} - \Delta_l a^\dagger_{2,\circlearrowleft}a_{2,\circlearrowleft} + J_0(a^\dagger_{1,\circlearrowleft}a_{2,\circlearrowleft} + a^\dagger_{2,\circlearrowleft}a_{1,\circlearrowleft})\\ &+ \omega_m b^\dagger b - g x_0 a^\dagger_{1,\circlearrowleft}a_{1,\circlearrowleft}(b + b^\dagger) + \mathrm{i}\varepsilon_l(a^\dagger_{1,\circlearrowleft} - a_{1,\circlearrowleft}). \quad (5)\end{aligned}$$

The comparison of Hamiltonians $\mathcal{H}_{\mathrm{f}}$ and $\mathcal{H}_{\mathrm{b}}$ shows that their detuning and coupling strengths are completely different due to the directional squeezing effect.

Below, we show that for our COM system, this directional squeezing effect leads to distinct changes in the radiation pressure in the mechanical mode, thereby resulting in a nonreciprocal phonon lasing action. Subsequently, for the forward-input case, the steady-state solutions can be obtained as follows (refer to Appendix for more details):

$$\begin{aligned}\alpha_{1,\circlearrowleft} &= \frac{\varepsilon_l(\kappa_2 - \mathrm{i}\Delta_s)}{(\kappa_1 - \mathrm{i}\Delta_l - \mathrm{i}g x_s)(\kappa_2 - \mathrm{i}\Delta_s) + J_s^2},\\ \alpha_{s,\circlearrowleft} &= \frac{J_s\alpha_{1,\circlearrowleft}}{\Delta_s + \mathrm{i}\kappa_2}, \quad \beta = \frac{g x_s|\alpha_{1,\circlearrowleft}|^2}{\omega_m - \mathrm{i}\gamma_m},\end{aligned} \quad (6)$$

where γ_m is the damping rate of the mechanical mode. In our calculations, for the backward-input case, we need to replace $\alpha_{1,\circlearrowleft}$, $\alpha_{s,\circlearrowleft}$, J_s, and Δ_s with $\alpha_{1,\circlearrowleft}$, $\alpha_{2,\circlearrowleft}$, J_0, and Δ_l, respectively. $x_s = x_0(\beta + \beta^*)$ is the steady-state mechanical displacement and is proportional to

$$x_s = \frac{\hbar g|\alpha_{1,\circlearrowleft}|^2}{m(\omega_m^2 + \gamma_m^2)}. \quad (7)$$

To determine the influence of the squeezing effect on the radiation pressure of the mechanical mode, we define the mechanical displacement amplification factor as follows:

$$\eta = \frac{x_s(\Lambda \neq 0)}{x_s(\Lambda = 0)}, \quad (8)$$

where $x_s(\Lambda \neq 0)$ ($x_s(\Lambda = 0)$) is the displacement corresponding to the forward-input case (backward-input case). Clearly, besides the driving field ε_l, the squeezing strength Λ affects the mechanical displacement values x_s. For the forward-input case, the effective coupling rate J_s and effective squeezed mode detuning Δ_s can be adjusted using the squeezing strength Λ. Figure 2 shows the mechanical displacement amplification factor η as a function of optical detuning Δ_l and squeezing strength Λ. The mechanical displacement amplification factor can be adjusted due to the squeezing effect; that is, the steady-state mechanical displacement x_s can be enhanced for the forward-input case. The amplified displacement indicates an enhancement in phonon generation [63, 64].

We now show that the nonreciprocal phonon lasing action can be achieved in our COM system. For the forward-input case, using the following supermode operator [14-16]:

$$a_\pm = (a_{1,\circlearrowleft} \pm a_{s,\circlearrowleft})/\sqrt{2}, \quad (9)$$

the Hamiltonian of eq. (3) can be written as follows:

$$\begin{aligned}H =& \omega_+ a^\dagger_+ a_+ + \omega_- a^\dagger_- a_- + \frac{\Delta}{2}(a^\dagger_+ a_- + a^\dagger_- a_+)\\ &+ \omega_m b^\dagger b - \frac{g x_0}{2}(a^\dagger_+ a_- b + b^\dagger a^\dagger_- a_+)\\ &+ \frac{\mathrm{i}\varepsilon_l}{\sqrt{2}}[(a^\dagger_+ + a^\dagger_-) - (a_+ + a_-)],\end{aligned} \quad (10)$$

after applying the rotating-wave approximation [14, 63, 64] with effective mode frequencies:

$$\omega_\pm = -(\Delta_s + \Delta_l)/2 \pm J_s, \quad (11)$$

and $\Delta = \Delta_s - \Delta_l$. For the backward-input case, $\Delta = 0$ and $J_s = J_0$. We note that compared with the traditional phonon laser system (absorption and emission of phonons are described using the fourth term) [14-16], eq. (10) contains an additional detuning term (third term), indicating that in the case of forward-input, the coupling between optical supermodes depends on the directional optical squeezing. Thus, the phonon lasing process can be dramatically modified. Usually, supermode operators are defined as $a_\pm = (a_{1,\circlearrowleft} \pm a_{s,\circlearrowleft})/\sqrt{2}$ for coupled cavities with the same resonant

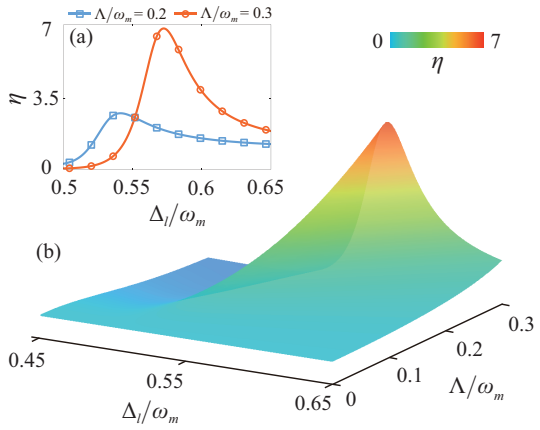

Figure 2 (Color online) (a) Mechanical displacement amplification factor η as a function of optical detuning Δ_l for different values of squeezing strength Λ. (b) η versus Δ_l and Λ with experimentally accessible parameter values $J_0/\omega_m = 0.5$ and $P_{\rm in} = 10\,\mu$W.

frequency [14, 15, 63, 64, 89]. As mentioned earlier, the squeezing strength Λ induces some changes in our system, such as the effective squeezed mode detuning Δ_s and effective coupling rate J_s. According to ref. [65], J_s is enhanced exponentially relative to J_0 with increasing Λ. However, in our study, to ensure that the transformation can be simplified safely, we do not consider the system to achieve strong coupling as we use the operators derived from eq. (3) to eq. (10). Hence, the maximum squeezing strength value is $0.3\omega_m$ in this study. For $\Lambda/\omega_m \leq 0.3$, we confirm that the detuning $\Delta = \Delta_s - \Delta_l$ and enhanced coupling rate $\Delta J = J_s - J_0$ are much smaller than Δ_l and J_0, respectively. For example, when $\Lambda/\omega_m = 0.3$, the detuning Δ/ω_m is approximately 0.1, and the enhanced coupling rate J_s/J_0 is approximately 1.05, indicating that our calculations are reasonable and valid.

Using the ladder and population inversion operators of the optical supermodes and following [14, 15]:

$$p = a_-^\dagger a_+, \quad \delta n = a_+^\dagger a_+ - a_-^\dagger a_-, \tag{12}$$

the motion equations of the system become

$$\begin{aligned} \dot{b} &= -(\gamma_m + \mathrm{i}\omega_m)b + \frac{\mathrm{i}gx_0}{2}p, \\ \dot{p} &= -2(\kappa_0 + \mathrm{i}J_s)p + \frac{\mathrm{i}}{2}(\Delta - gx_0 b)\delta n + \frac{\varepsilon_l}{\sqrt{2}}(a_+ + a_-^\dagger), \end{aligned} \tag{13}$$

where $\kappa_0 = (\kappa_1 + \kappa_2)/2$. Following the standard procedures (more details in Appendix A2), the mechanical gain G can be obtained as follows:

$$\begin{aligned} G = G_0 + \mathcal{G} = &\frac{g^2 x_0^2 \kappa_0 \delta n}{2(2J_s - \omega_m)^2 + 8\kappa_0^2} \\ &+ \frac{\varepsilon_l^2 g^2 x_0^2 (\omega_m - 2J_s)(\Delta_s + \Delta_l)\kappa_0}{\left[4(2J_s - \omega_m)^2 + 16\kappa_0^2\right]\left[D^2 + (\Delta_l + \Delta_s)^2\kappa_0^2\right]}, \end{aligned} \tag{14}$$

with

$$\begin{aligned} D &= J_s^2 + \kappa_0^2 - \Delta_s\Delta_l + \frac{[g^2 x_0^2 n_b - 2gx_0\Delta\mathrm{Re}(b)]}{4}, \\ deltan &= \frac{\varepsilon_l^2\,[2J_s\Delta_s - \kappa_0 g x_0 \mathrm{Im}(b) - J_s g x_0 \mathrm{Re}(b)]}{D^2 + \kappa_0^2(\Delta_l + \Delta_s)^2}, \end{aligned} \tag{15}$$

where $n_b = b^\dagger b$ is the phonon number. We note that the first term G_0 in eq. (14) is proportional to the population inversion δn, and δn depends on Δ_s, which is quite different from the conventional phonon laser system without the directional quantum squeezing effect. Additionally, the second term $\mathcal{G}$ in eq. (14) depends on Δ_s, indicating that different mechanical gains can be obtained for the forward-input and backward-input cases, which enables achieving a nonreciprocal phonon laser.

3 Nonreciprocal phonon laser

In numerical simulations, to demonstrate that the observation of the phonon lasing process is within the current experimental reach, we select experimentally feasible parameters [14], i.e., $\omega_a/2\pi = 30.7$ THz, the optical quality factors $Q_1 = 9.7 \times 10^7$ and $Q_2 = 4 \times 10^7$, $\kappa_{1,2} = \omega_a/Q_{1,2}$, $2r_1 = 66\,\mu$m, $2r_2 = 69\,\mu$m, $\omega_m/2\pi = 23.4$ MHz, $m = 50$ ng, $\gamma_m = 0.24$ MHz, and $\Lambda/\omega_m = 0.3$; thus, $\Delta/\omega_m \sim 0.1$ and $J_s/J_0 \sim 1.05$.

In Figure 3(a), the calculated mechanical gain G is plotted as a function of the optical detuning Δ_l and coupling strength J_0 for the forward-input case. Notably, for $\Lambda/\omega_m = 0.3$, the mechanical gain $G/\gamma_m > 1$ can be obtained via the proper selection of Δ_l and J_0, indicating that the system operates in the phonon lasing regime. A maximum mechanical gain of $G/\gamma_m \simeq 2.7$ is obtained with $\Delta_l/\omega_m \sim 0.545$ and $J_0/\omega_m \sim 0.48$. When $\omega_m = \omega_+ - \omega_- = 2J_s$, $\Delta_l/\omega_m = 0.545$ corresponds to driving up the supermode and produces the maximum population inversion, indicating that the strongest phonon lasing occurs due to the resonance of the input drive field with the supermode ω_+ (i.e., driving up the energy level in Figure 1(d); refer to refs. [14-16]). Under this condition, when the upper state is sufficiently populated by the driving laser, population inversion can be realized; thus, the transition from the upper state to the lower state occurs, accompanied by phonon emissions (i.e., phonon lasing). In Figure 3(b)-(d), we plot the dependence of mechanical gain G on the input directions of the driving field. For the backward-input case, the maximum is located at $\Delta_l/\omega_m \sim 0.475$, corresponding to a backward phonon laser (Figure 3(a)). However, for the forward-input case, the squeezing effect leads to a blueshift in the maximum mechanical gain G (orange dashed curve in Figure 3(c) and red solid curve in Figure 3(d)). In

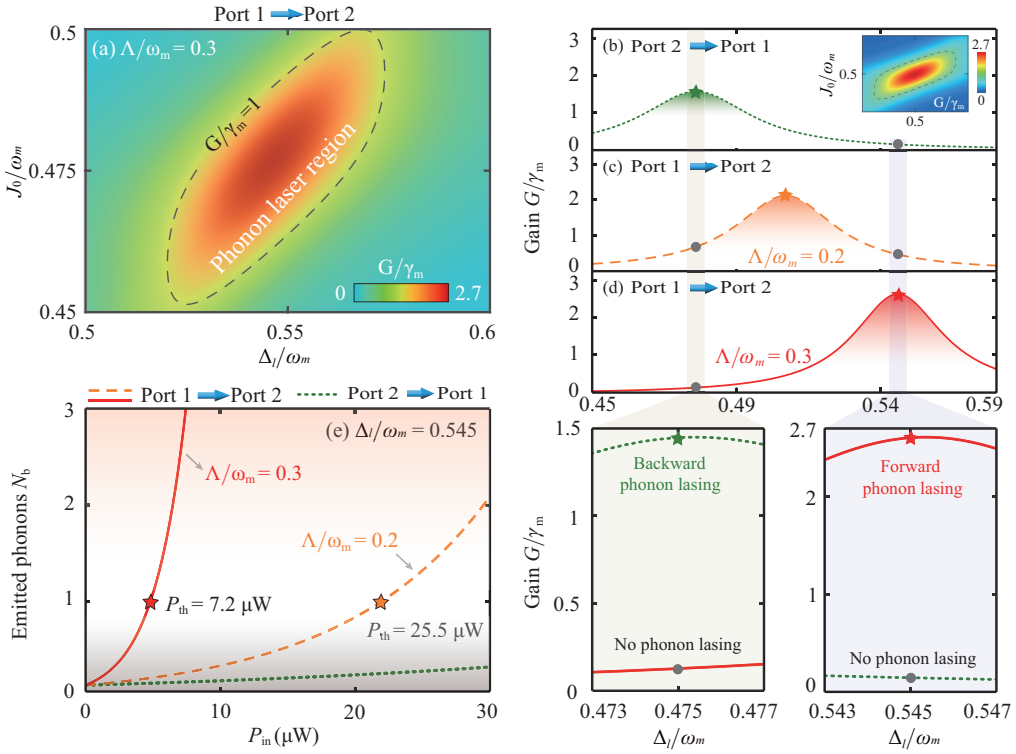

Figure 3 (Color online) (a) Mechanical gain G versus detuning Δ_l and coupling strength J_0 for the forward-input case (port 1→ port 2). (b)-(d) G versus Δ_l for different input directions. The right inset shows G versus Δ_l and J_0 for the backward-input case (port 2→ port 1). The orange dashed and red solid curves correspond to the forward-input case for squeezing strengths $\Lambda/\omega_m = 0.2$ and $\Lambda/\omega_m = 0.3$, respectively. The green dashed curve corresponds to the backward-input case for $\Lambda/\omega_m = 0.2$ and $\Lambda/\omega_m = 0.3$. (e) Stimulated emitted phonon number N_b as a function of pump power $P_{\rm in}$ for different input directions. The five-pointed stars correspond to the threshold power $P_{\rm th}$, which is determined using the threshold condition $G = \gamma_m$. We select $P_{\rm in} = 10\,\mu$W in (a)-(d), $J_0/\omega_m = 0.48$ in (b)-(d), and $\Delta_l/\omega_m = 0.545$ in (e).

other words, for $\Lambda/\omega_m = 0.3$, by driving the system from the left side (Port 1 → Port 2), we obtain the maximum mechanical gain at $\Delta_l/\omega_m \sim 0.545$ (Figure 3(c)), corresponding to a forward phonon laser.

The underlying physical mechanism can be explained as follows: in the forward-input case, the squeezing effect causes a frequency shift to $a_{s,\circlearrowleft}$ with respect to the bare mode $a_{2,\circlearrowleft}$ [65], leading to $G/\gamma_m > 1$ at approximately $\Delta_l/\omega_m \sim 0.545$. By contrast, in the backward-input case, the squeezing effect does not contribute anything to $a_{2,\circlearrowleft}$, corresponding to a conventional phonon laser (i.e., $G/\gamma_m > 1$ at approximately $\Delta_l/\omega_m \sim 0.475$ with $J_0/\omega_m = 0.48$) [14-16]. This implies that by adjusting the detuning Δ_l and squeezing strength Λ, substantially enhanced or suppressed mechanical gain can be obtained by driving the device from the left side to the right side, or *vice versa*. Thus, our system provides a new route to realize a nonreciprocal phonon laser by changing the input directions. Compared with the method of using a rotating cavity to realize a nonreciprocal phonon laser [63, 64], our scheme requires only two-mode matching in one resonator without high-speed rotation and is therefore easier to conduct experiments on. Thus, this study proposes a new way to realize a nonreciprocal phonon laser. According to eq. (14), the stimulated emitted phonon number N_b can be calculated as follows:

$$N_b = \exp[2(G - \gamma_m)/\gamma_m], \tag{16}$$

which characterizes the performance of the phonon laser [14]. Subsequently, from eq. (16) and under the threshold condition of the phonon laser $N_b = 1$ (i.e., $G = \gamma_m$) [14], we derive the threshold pump power as follows:

$$P_{\rm th} \approx \frac{2\hbar\kappa_0\gamma_m\omega_l[(J_s^2 + \kappa_0^2 - \Delta_l\Delta_s)^2 + \kappa_0^2(\Delta_s + \Delta_l)^2]}{\kappa_1 J_s g^2 x_0^2 \Delta_s}, \tag{17}$$

where we use $|b_s|^2 \ll 1$ at the threshold power. The directional quantum squeezing effect considerably affects the threshold power $P_{\rm th}$. Figure 3(e) shows the stimulated emitted phonon number N_b as a function of the pump power $P_{\rm in}$. For the forward-input case (i.e., $\Lambda/\omega_m = 0.3$), the threshold power is approximately 7.2 μW at a fixed $\Delta_l/\omega_m = 0.545$ (corresponding to the maximum mechanical gain shown in Figure 3(d)), which approaches the threshold power at approximately 7 μW, which is also obtained in experiments [14]. In comparison, for the backward-input case (without the squeezing effect), the mechanical gain is

suppressed at $\Delta_l/\omega_m = 0.545$; thus, much higher threshold power is required to implement the phonon laser.

To clearly see the squeezing effect on the nonreciprocal phonon lasing action, we introduce the following isolation parameter:

$$\mathcal{R} = 10\log_{10}\frac{N_b(\Lambda \neq 0)}{N_b(\Lambda = 0)}, \tag{18}$$

where $N_b\,(\Lambda \neq 0)$ (or $N_b\,(\Lambda = 0)$) is the emitted phonon number corresponding to the forward-input case (or backward-input case). Figure 4(a) shows the isolation parameter $\mathcal{R}$ versus the optical detuning Δ_l and squeezing strength Λ. A nonzero isolation parameter $\mathcal{R}$ indicates that nonreciprocity occurs in the phonon lasing action. When the detuning regions are selected correctly, nonreciprocity occurs. For example, for the detuning of $\Delta_l/\omega_m \sim 0.545$ and squeezing strength of $\Lambda/\omega_m = 0.3$, forward phonon lasing can be realized (Figure 3(b) and (d)), which is an inevitable result due to the difference between $\delta n\,(\Lambda \neq 0)$ and $\delta n\,(\Lambda = 0)$. Thus, in such a COM system, nonreciprocal phonon lasing can be realized by directional quantum squeezing. In the experiments, the decay rate of the photon modes can be engineered, for example, by placing an external nanotip near a microresonator [102]. The effect of the normalized decay rate of the photon mode κ/κ_0 on the optimum mechanical gain G for different input directions is shown in Figure 4(b). For the same optical decay rate value κ/κ_0, the optimum mechanical gain G for the forward-input case can reach a much higher value than that for the opposite direction due to the directional quantum squeezing. This implies that for the forward phonon laser, the mechanical gain exhibits squeezing-enhanced robustness against optical decays.

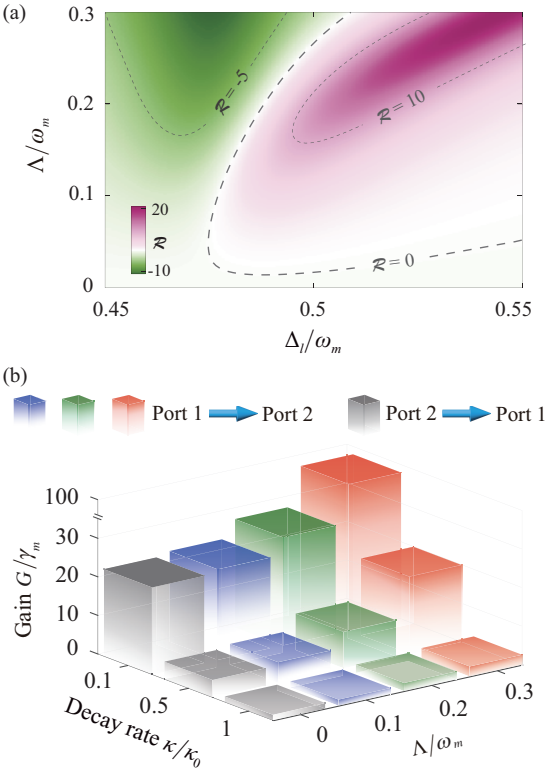

Figure 4 (Color online) (a) Dependence of the isolation parameter $\mathcal{R}$ on the detuning Δ_l and squeezing strength Λ. (b) Optimum mechanical gain G versus scaled decay rate κ/κ_0 and squeezing strength Λ for different input directions with the experimentally accessible parameter values $J_0/\omega_m = 0.48$ and $P_{\rm in} = 10\,\mu$W.

4 Experimental feasibility

Phonon lasers have been experimentally achieved in various physical systems [9, 11-24]. In particular, optically pumped phonon lasing has been demonstrated in a compound COM system comprising two coupled silica WGM microtoroid resonators and a nearby optical fiber [14-16]. As confirmed in an experiment [14], the first resonator (with a diameter of $d_1 = 66\,\mu$m) supports a high Q ($Q_1 = 9.7\times10^7$) optical WGM and a mechanical mode with a mechanical quality factor of $Q_m = 1\times10^3$ and a resonant frequency of $\omega_m/2\pi = 23.4$ MHz. The second resonator (with a diameter of $d_2 = 69\,\mu$m) supports a pure optical WGM with an optical quality factor of $Q_2 = 4\times10^7$. By placing a tapered optical fiber near the first resonator, a tunable laser can be coupled to R_1 via the optical evanescent field. Furthermore, the two resonators can be coupled by the evanescent field, and the coupling strength J_0 can be adjusted by controlling the air gap between the resonators. For a controllable gap of 0.2-2 μm, J_0 is typically between 5 MHz-5 GHz [14]. In such a COM system, when the upper state (supermode ω_+) is occupied by a sufficient number of photons coming from the driving laser through the nearby optical waveguide, these photons begin to split into the lower-frequency photons of the lower state (supermode ω_-) and coherent phonons (i.e., phonon lasing) [14]. As shown in Table 1, we compare the experimental performance of the recent phonon laser based on a composite COM system comprising two coupled silica microtoroid resonators and a nearby optical waveguide [14-16].

Recently, due to advances in experimental manufacturing [90-101], microring resonators with large $\chi^{(2)}$ nonlinearity and high Q have been fabricated using various thin film materials, such as silicon nitride, lithium niobate, and aluminum nitride. Table 2 shows more relevant parameters required for experimentally achieving a $\chi^{(2)}$-nonlinear optical resonator. We note that the Q factors of lithium niobate-based resonators can reach 10^7 or 10^8 [90, 91, 93], which are better suited for our study. For an experimentally feasible quality factor of $Q \simeq 4\times10^7$, the decay rate of a resonator with frequency $\omega_a/2\pi = 30.7$ THz is $\kappa \simeq 48.2$ MHz. According to eq. (a8) (Appendix), the relationship between the power P_p

Table 1 Experimental parameters of phonon laser in a coupled-microtoroid COM system

References	Resonators (Material)	Geometry	Diameter (μm)	Optical quality factors	Mechanical frequency (MHz)	Mechanical quality factors	Power threshold (μW)
[14]	R_1 (Si)	microtoroid	~66	9.7×10^7	147.1	1×10^3	7
	R_2 (Si)	microtoroid	~69	3×10^7	–	–	
[15]	R_1 (Si)	microtoroid	~68	9.25×10^7	59.2	18×10^3	1.2
	R_2 (Si)	microtoroid	~69	2.5×10^7	–	–	
[16]	R_1 (Si)	microtoroid	~34.5	6.33×10^7	17.38	0.4×10^3	2.5
	R_2 (Si)	microtoroid	~34	1.5×10^7	–	–	

Table 2 Performance of various $\chi^{(2)}$ nonlinearity integrated media. PPLN: periodically poled $LiNbO_3$

References	Material	$\chi^{(2)}$ (pm/V)	Geometry	Size (μm): rings: $r/w/h$, disks: r/h, and spheres: r	Optical quality factor	Nonlinear single-photon coupling strength (MHz)	Pump power (mW)
[90]	PPLN	0.023	microdisk	1500/500	2.0×10^8	–	25
[91]	$LiNbO_3$	–	microtoroid	1900/500	3.4×10^7	–	0.03
[92]	AlN	1.3	microring	30/1.12/1.0	1.8×10^5	0.74	24.4
[93]	$LiNbO_3$	2.1	microdisk	51/0.7	1.1×10^5	–	10
[94]	SiO_2	–	microsphere	62	4.8×10^7	–	0.9
[95]	AlN	6	microring	60/1.2/1.0	1.0×10^6	0.5	11
[96]	AlN	27	microring	55/1.6/2	2.6×10^5	–	0.35
[97]	Si_3N_4	0.2	microring	23/1.2/0.6	1.2×10^6	–	15
[98]	Si_3N_4	–	microring	23/1.2/1.1	1.38×10^6	0.25	22.4
[99]	$LiNbO_3$	0.6	microring	80/1.6/0.6	9.0×10^5	–	20
[100]	PPLN	40	microring	–	6.0×10^5	7.4	0.03
[101]	PPLN	–	microring	75/–/–	1.8×10^6	1.2	0.1

of a pump field and squeezing strength Λ can be expressed as follows [65, 89]:

$$\Lambda = \sqrt{8g_d^2\kappa_2 P_p/\hbar\omega_p\kappa_p^2}, \tag{19}$$

where g_d denotes the nonlinear single-photon coupling strength in the parametric nonlinear process and κ_p denotes the external decay rate for the pump field. We select the following experimentally feasible values [90-101]: $g_d = 0.025\,\mathrm{MHz}$, $\kappa_2 = 48.2\,\mathrm{MHz}$, $\kappa_p = 2\kappa_2$, and $\omega_p = 2\omega_a$. We choose pump power $P_p = 0.02\,\mu\mathrm{W}$ or $P_p = 30\,\mathrm{mW}$ such that it leads to $\Lambda/\omega_m \sim 0.2$ or $\Lambda/\omega_m \sim 290$. Therefore, we strongly believe that our proposed scheme is experimentally feasible.

5 Conclusion

In conclusion, we studied the nonreciprocal phonon laser based on a compound COM system comprising an optomechanical resonator and a nonlinear optical resonator. By unidirectionally pumping the nonlinear optical resonator, the squeezed effect occurs only in the selected direction, which substantially modifies the mechanical gain and power threshold, resulting in nonreciprocal phonon lasing. Moreover, we find that in such nonreciprocal devices, the mechanical gain exhibits squeezing-enhanced robustness against optical decays. Our results open up a new route to manipulate COM devices or other acoustic devices using directional quantum squeezing, and find intriguing applications in designing phonon chips or high-precision motion sensors [36, 37, 103]. Furthermore, our scheme opens up many possibilities for further research: studying the role of directional quantum squeezing in enhancing or steering, for example, photon or phonon blockade [104, 105], macroscopic entanglement [106, 107], and backscattering-immune force sensing [5], by including quantum noise terms.

Hui Jing was supported by the National Natural Science Foundation of China (Grant No. 11935006), the Hunan Provincial Major Sci-Tech Program (Grant No. 2023ZJ1010), and the Science and Technology Innovation Program of Hunan Province (Grant No. 2020RC4047). Le-Man Kuang was supported by the National Natural Science Foundation of China (Grant Nos. 12247105, 12175060, and 11935006), and XJ-Lab Key Project (Grant No. 23XJ02001). Keyu Xia was supported by the National Key R&D Program of China (Grant No. 2019YFA0308704), the National Natural Science Foundation of China (Grant No. 92365107), and the Program for Innovative Talents and Teams in Jiangsu (Grant No. JSSCTD202138). Tian-Xiang Lu is supported by the National Natural Science Foundation of China (Grant No. 12205054), the Jiangxi Provincial Education Office Natural Science Fund Project (Grant No. GJJ211437), and the Ph.D. Research Foundation (Grant No. BSJJ202122). Xing Xiao was supported by the National Natural Science Foundation of China (Grant No. 12265004). Yan Wang was supported by the National Natural Science Foundation of China (Grant No. 12205256), and the Henan Provincial Science and Technology Research Project (Grant

No. 232102221001).

Conflict of interest The authors declare that they have no conflict of interest.

1 L. J. Swenson, A. Cruciani, A. Benoit, M. Roesch, C. S. Yung, A. Bideaud, and A. Monfardini, Appl. Phys. Lett. **96**, 263511 (2010), arXiv: 1004.5066.
2 H. Shin, J. A. Cox, R. Jarecki, A. Starbuck, Z. Wang, and P. T. Rakich, Nat. Commun. **6**, 6427 (2015), arXiv: 1409.0580.
3 A. Ganesan, C. Do, and A. Seshia, Phys. Rev. Lett. **118**, 033903 (2017), arXiv: 1704.08008.
4 J. D. Cohen, S. M. Meenehan, G. S. MacCabe, S. Gröblacher, A. H. Safavi-Naeini, F. Marsili, M. D. Shaw, and O. Painter, Nature **520**, 522 (2015), arXiv: 1410.1047.
5 Y. He, Z. Feng, Y. Jing, W. Xiong, X. Chen, T. Kuang, G. Xiao, Z. Tan, and H. Luo, Opt. Express **31**, 37507 (2023).
6 M. Serra-Garcia, V. Peri, R. Süsstrunk, O. R. Bilal, T. Larsen, L. G. Villanueva, and S. D. Huber, Nature **555**, 342 (2018), arXiv: 1708.05015.
7 N. Li, J. Ren, L. Wang, G. Zhang, P. Hänggi, and B. Li, Rev. Mod. Phys. **84**, 1045 (2012), arXiv: 1108.6120.
8 R. Huang, and H. Jing, Nat. Photon. **13**, 372 (2019), arXiv: 1907.01211.
9 K. Vahala, M. Herrmann, S. Knünz, V. Batteiger, G. Saathoff, T. W. Hänsch, and T. Udem, Nat. Phys. **5**, 682 (2009).
10 T. Behrle, T. L. Nguyen, F. Reiter, D. Baur, B. de Neeve, M. Stadler, M. Marinelli, F. Lancellotti, S. F. Yelin, and J. P. Home, Phys. Rev. Lett. **131**, 043605 (2023), arXiv: 2301.08156.
11 J. T. Mendonça, H. Terças, G. Brodin, and M. Marklund, Europhys. Lett. **91**, 33001 (2010), arXiv: 0911.4916.
12 T. Kuang, R. Huang, W. Xiong, Y. Zuo, X. Han, F. Nori, C. W. Qiu, H. Luo, H. Jing, and G. Xiao, Nat. Phys. **19**, 414 (2023), arXiv: 2210.06137.
13 R. M. Pettit, W. Ge, P. Kumar, D. R. Luntz-Martin, J. T. Schultz, L. P. Neukirch, M. Bhattacharya, and A. N. Vamivakas, Nat. Photon. **13**, 402 (2019).
14 I. S. Grudinin, H. Lee, O. Painter, and K. J. Vahala, Phys. Rev. Lett. **104**, 083901 (2010), arXiv: 0907.5212.
15 G. Wang, M. Zhao, Y. Qin, Z. Yin, X. Jiang, and M. Xiao, Photon. Res. **5**, 73 (2017).
16 J. Zhang, B. Peng, Ş. K. Özdemir, K. Pichler, D. O. Krimer, G. Zhao, F. Nori, Y. Liu, S. Rotter, and L. Yang, Nat. Photon. **12**, 479 (2018).
17 L. Mercadé, K. Pelka, R. Burgwal, A. Xuereb, A. Martínez, and E. Verhagen, Phys. Rev. Lett. **127**, 073601 (2021), arXiv: 2101.10788.
18 J. Sheng, X. Wei, C. Yang, and H. Wu, Phys. Rev. Lett. **124**, 053604 (2020), arXiv: 2004.09154.
19 Q. Zhang, C. Yang, J. Sheng, and H. Wu, Proc. Natl. Acad. Sci. USA **119**, e2207543119 (2022).
20 I. Mahboob, K. Nishiguchi, A. Fujiwara, and H. Yamaguchi, Phys. Rev. Lett. **110**, 127202 (2013).
21 A. J. Kent, R. N. Kini, N. M. Stanton, M. Henini, B. A. Glavin, V. A. Kochelap, and T. L. Linnik, Phys. Rev. Lett. **96**, 215504 (2006).
22 R. P. Beardsley, A. V. Akimov, M. Henini, and A. J. Kent, Phys. Rev. Lett. **104**, 085501 (2010).
23 J. Kabuss, A. Carmele, T. Brandes, and A. Knorr, Phys. Rev. Lett. **109**, 054301 (2012).
24 A. Khaetskii, V. N. Golovach, X. Hu, and I. Žutić, Phys. Rev. Lett. **111**, 186601 (2013), arXiv: 1306.1786.
25 N. Wang, H. Wen, J. C. Alvarado Zacarias, J. E. Antonio-Lopez, Y. Zhang, D. Cruz Delgado, P. Sillard, A. Schülzgen, B. E. A. Saleh, R. Amezcua-Correa, and G. Li, Sci. Adv. **9**, eadg7841 (2023).
26 M. Aspelmeyer, T. J. Kippenberg, and F. Marquardt, Rev. Mod. Phys. **86**, 1391 (2014), arXiv: 1303.0733.
27 H. Jing, S. K. Özdemir, X. Y. Lü, J. Zhang, L. Yang, and F. Nori, Phys. Rev. Lett. **113**, 053604 (2014), arXiv: 1403.0657.
28 Y. F. Xie, Z. Cao, B. He, and Q. Lin, Opt. Express **28**, 22580 (2020).
29 H. Lü, S. K. Özdemir, L. M. Kuang, F. Nori, and H. Jing, Phys. Rev. Appl. **8**, 044020 (2017), arXiv: 1701.08000.
30 Y. L. Zhang, C. L. Zou, C. S. Yang, H. Jing, C. H. Dong, G. C. Guo, and X. B. Zou, New J. Phys. **20**, 093005 (2018), arXiv: 1706.02097.
31 X. Y. Zhang, C. Cao, Y. P. Gao, L. Fan, R. Zhang, and C. Wang, New J. Phys. **25**, 053039 (2023).
32 B. Wang, Z. X. Liu, X. Jia, H. Xiong, and Y. Wu, Commun. Phys. **1**, 43 (2018).
33 B. Wang, H. Xiong, X. Jia, and Y. Wu, Sci. Rep. **8**, 282 (2018).
34 B. He, L. Yang, and M. Xiao, Phys. Rev. A **94**, 031802 (2016), arXiv: 1609.00075.
35 Q. Lin, B. He, and M. Xiao, Phys. Rev. Res. **3**, L032018 (2021), arXiv: 2101.05237.
36 S. Kim, X. Xu, J. M. Taylor, and G. Bahl, Nat. Commun. **8**, 205 (2017), arXiv: 1609.08674.
37 H. Xu, L. Jiang, A. A. Clerk, and J. G. E. Harris, Nature **568**, 65 (2019), arXiv: 1807.03484.
38 D. G. Lai, J. F. Huang, X. L. Yin, B. P. Hou, W. Li, D. Vitali, F. Nori, and J. Q. Liao, Phys. Rev. A **102**, 011502 (2020), arXiv: 2007.14851.
39 R. Fleury, D. L. Sounas, C. F. Sieck, M. R. Haberman, and A. Alú, Science **343**, 516 (2014).
40 B. I. Popa, and S. A. Cummer, Nat. Commun. **5**, 3398 (2014).
41 J. Zhang, B. Peng, Ş. K. Özdemir, Y. Liu, H. Jing, X. Lü, Y. Liu, L. Yang, and F. Nori, Phys. Rev. B **92**, 115407 (2015), arXiv: 1510.07343.
42 T. Devaux, V. Tournat, O. Richoux, and V. Pagneux, Phys. Rev. Lett. **115**, 234301 (2015), arXiv: 1510.06633.
43 A. Seif, W. DeGottardi, K. Esfarjani, and M. Hafezi, Nat. Commun. **9**, 1207 (2018), arXiv: 1710.08967.
44 B. Liang, X. S. Guo, J. Tu, D. Zhang, and J. C. Cheng, Nat. Mater. **9**, 989 (2010).
45 L. Shao, W. Mao, S. Maity, N. Sinclair, Y. Hu, L. Yang, and M. Lončar, Nat. Electron. **3**, 267 (2020).
46 C. Coulais, D. Sounas, and A. Alú, Nature **542**, 461 (2017), arXiv: 1704.03305.
47 Y. Li, C. Shen, Y. Xie, J. Li, W. Wang, S. A. Cummer, and Y. Jing, Phys. Rev. Lett. **119**, 035501 (2017).
48 Q. Wang, Z. Zhou, D. Liu, H. Ding, M. Gu, and Y. Li, Sci. Adv. **8**, eabq4451 (2022).
49 G. Penelet, V. Pagneux, G. Poignand, C. Olivier, and Y. Aurégan, Phys. Rev. Appl. **16**, 064012 (2021).
50 X. F. Li, X. Ni, L. Feng, M. H. Lu, C. He, and Y. F. Chen, Phys. Rev. Lett. **106**, 084301 (2011).
51 A. V. Poshakinskiy, and A. N. Poddubny, Phys. Rev. Lett. **118**, 156801 (2017), arXiv: 1611.07970.
52 B. Li, Nat. Mater. **9**, 962 (2010).
53 S. A. Cummer, Science **343**, 495 (2014).
54 Y. Wang, B. Yousefzadeh, H. Chen, H. Nassar, G. Huang, and C. Daraio, Phys. Rev. Lett. **121**, 194301 (2018), arXiv: 1803.11503.
55 R. Fleury, A. B. Khanikaev, and A. Alú, Nat. Commun. **7**, 11744 (2016), arXiv: 1511.08427.
56 S. Manipatruni, J. T. Robinson, and M. Lipson, Phys. Rev. Lett. **102**, 213903 (2009).
57 Z. Shen, Y. L. Zhang, Y. Chen, C. L. Zou, Y. F. Xiao, X. B. Zou, F. W. Sun, G. C. Guo, and C. H. Dong, Nat. Photon. **10**, 657 (2016), arXiv: 1604.02297.
58 F. Ruesink, M. A. Miri, A. Alú, and E. Verhagen, Nat. Commun. **7**, 13662 (2016), arXiv: 1607.07180.
59 F. Ruesink, J. P. Mathew, M. A. Miri, A. Alú, and E. Verhagen, Nat. Commun. **9**, 1798 (2018), arXiv: 1708.07792.
60 Z. Shen, Y. L. Zhang, Y. Chen, Y. F. Xiao, C. L. Zou, G. C. Guo, and C. H. Dong, Phys. Rev. Lett. **130**, 013601 (2023).
61 N. R. Bernier, L. D. Tóth, A. Koottandavida, M. A. Ioannou, D. Malz, A. Nunnenkamp, A. K. Feofanov, and T. J. Kippenberg, Nat. Commun. **8**, 604 (2017), arXiv: 1612.08223.
62 Z. Shen, Y. L. Zhang, Y. Chen, F. W. Sun, X. B. Zou, G. C. Guo,

C. L. Zou, and C. H. Dong, Nat. Commun. **9**, 1797 (2018), arXiv: 1709.06236.
63 Y. Jiang, S. Maayani, T. Carmon, F. Nori, and H. Jing, Phys. Rev. Appl. **10**, 064037 (2018), arXiv: 1810.08761.
64 Y. Xu, J. Y. Liu, W. Liu, and Y. F. Xiao, Phys. Rev. A **103**, 053501 (2021).
65 L. Tang, J. Tang, M. Chen, F. Nori, M. Xiao, and K. Xia, Phys. Rev. Lett. **128**, 083604 (2022), arXiv: 2110.05016.
66 X. Y. Lü, Y. Wu, J. R. Johansson, H. Jing, J. Zhang, and F. Nori, Phys. Rev. Lett. **114**, 093602 (2015), arXiv: 1412.2864.
67 W. Qin, V. Macrí, A. Miranowicz, S. Savasta, and F. Nori, Phys. Rev. A **100**, 062501 (2019), arXiv: 1902.04216.
68 W. Qin, A. Miranowicz, P. B. Li, X. Y. Lü, J. Q. You, and F. Nori, Phys. Rev. Lett. **120**, 093601 (2018), arXiv: 1709.09555.
69 W. Zhao, S. D. Zhang, A. Miranowicz, and H. Jing, Sci. China-Phys. Mech. Astron. **63**, 224211 (2020), arXiv: 1905.12493.
70 Y. Wang, C. Li, E. M. Sampuli, J. Song, Y. Jiang, and Y. Xia, Phys. Rev. A **99**, 023833 (2019), arXiv: 1902.05751.
71 C. J. Zhu, L. L. Ping, Y. P. Yang, and G. S. Agarwal, Phys. Rev. Lett. **124**, 073602 (2020), arXiv: 1907.00522.
72 Y. Wang, J. L. Wu, J. Song, Z. J. Zhang, Y. Y. Jiang, and Y. Xia, Phys. Rev. A **101**, 053826 (2020).
73 Y. Wang, J. L. Wu, J. X. Han, Y. Y. Jiang, Y. Xia, and J. Song, Phys. Rev. A **102**, 032601 (2020), arXiv: 2008.05670.
74 W. Qin, A. Miranowicz, H. Jing, and F. Nori, Phys. Rev. Lett. **127**, 093602 (2021), arXiv: 2101.03662.
75 Y. H. Chen, W. Qin, X. Wang, A. Miranowicz, and F. Nori, Phys. Rev. Lett. **126**, 023602 (2021), arXiv: 2008.04078.
76 M. Villiers, W. C. Smith, A. Petrescu, A. Borgognoni, M. Delbecq, A. Sarlette, M. Mirrahimi, P. Campagne-Ibarcq, T. Kontos, and Z. Leghtas, arXiv: 2212.04991.
77 W. Ge, B. C. Sawyer, J. W. Britton, K. Jacobs, J. J. Bollinger, and M. Foss-Feig, Phys. Rev. Lett. **122**, 030501 (2019).
78 S. C. Burd, R. Srinivas, H. M. Knaack, W. Ge, A. C. Wilson, D. J. Wineland, D. Leibfried, J. J. Bollinger, D. T. C. Allcock, and D. H. Slichter, Nat. Phys. **17**, 898 (2021), arXiv: 2009.14342.
79 P. B. Li, Y. Zhou, W. B. Gao, and F. Nori, Phys. Rev. Lett. **125**, 153602 (2020), arXiv: 2003.07151.
80 M. A. Lemonde, N. Didier, and A. A. Clerk, Nat. Commun. **7**, 11338 (2016), arXiv: 1509.09238.
81 Y. Wang, J. L. Wu, J. X. Han, Y. Xia, Y. Y. Jiang, and J. Song, Phys. Rev. Appl. **17**, 024009 (2022), arXiv: 2112.08562.
82 X. F. Pan, X. L. Hei, X. L. Dong, J. Q. Chen, C. P. Shen, H. Ali, and P. B. Li, Phys. Rev. A **107**, 023722 (2023), arXiv: 2210.04751.
83 X. L. Hei, P. B. Li, X. F. Pan, and F. Nori, Phys. Rev. Lett. **130**, 073602 (2023), arXiv: 2301.10424.
84 Y. Wang, H. L. Zhang, J. L. Wu, J. Song, K. Yang, W. Qin, H. Jing, and L. M. Kuang, Sci. China-Phys. Mech. Astron. **66**, 110311 (2023), arXiv: 2307.11961.
85 Y.-F. Jiao, Y.-L. Zuo, Y. Wang, W. Lu, J.-Q. Liao, L.-M. Kuang, and H. Jing, arXiv: 2311.11484.
86 C. P. Shen, J. Q. Chen, X. F. Pan, Y. M. Ren, X. L. Dong, X. L. Hei, Y. F. Qiao, and P. B. Li, Phys. Rev. A **108**, 023716 (2023).
87 D. Y. Wang, L. L. Yan, S. L. Su, C. H. Bai, H. F. Wang, and E. Liang, Opt. Express **31**, 22343 (2023).
88 D. W. Liu, K. W. Huang, Y. Wu, and L. G. Si, Appl. Phys. Lett. **123**, 061103 (2023).
89 K. W. Huang, Y. Wu, and L. G. Si, Opt. Lett. **47**, 3311 (2022).
90 V. S. Ilchenko, A. A. Savchenkov, A. B. Matsko, and L. Maleki, Phys. Rev. Lett. **92**, 043903 (2004).
91 J. U. Fürst, D. V. Strekalov, D. Elser, M. Lassen, U. L. Andersen, C. Marquardt, and G. Leuchs, Phys. Rev. Lett. **104**, 153901 (2010), arXiv: 0912.3864.
92 X. Guo, C. L. Zou, H. Jung, and H. X. Tang, Phys. Rev. Lett. **117**, 123902 (2016).
93 J. Lin, Y. Xu, J. Ni, M. Wang, Z. Fang, L. Qiao, W. Fang, and Y. Cheng, Phys. Rev. Appl. **6**, 014002 (2016).
94 X. Zhang, Q. T. Cao, Z. Wang, Y. Liu, C. W. Qiu, L. Yang, Q. Gong, and Y. F. Xiao, Nat. Photon. **13**, 21 (2019).
95 A. W. Bruch, X. Liu, J. B. Surya, C. L. Zou, and H. X. Tang, Optica **6**, 1361 (2019), arXiv: 1909.07422.
96 Z. Ma, J. Y. Chen, Z. Li, C. Tang, Y. M. Sua, H. Fan, and Y. P. Huang, Phys. Rev. Lett. **125**, 263602 (2020), arXiv: 2010.04242.
97 X. Lu, G. Moille, A. Rao, D. A. Westly, and K. Srinivasan, Nat. Photon. **15**, 131 (2021), arXiv: 2003.12176.
98 J. Q. Wang, Y. H. Yang, M. Li, X. X. Hu, J. B. Surya, X. B. Xu, C. H. Dong, G. C. Guo, H. X. Tang, and C. L. Zou, Phys. Rev. Lett. **126**, 133601 (2021), arXiv: 2011.10352.
99 Y. Xu, A. A. Sayem, L. Fan, C. L. Zou, S. Wang, R. Cheng, W. Fu, L. Yang, M. Xu, and H. X. Tang, Nat. Commun. **12**, 4453 (2021), arXiv: 2012.14909.
100 J. Lu, A. Al Sayem, Z. Gong, J. B. Surya, C. L. Zou, and H. X. Tang, Optica **8**, 539 (2021), arXiv: 2101.04735.
101 J. Lu, M. Li, C. L. Zou, A. Al Sayem, and H. X. Tang, Optica **7**, 1654 (2020), arXiv: 2007.07411.
102 B. Peng, Ş. K. Özdemir, S. Rotter, H. Yilmaz, M. Liertzer, F. Monifi, C. M. Bender, F. Nori, and L. Yang, Science **346**, 328 (2014), arXiv: 1410.7474.
103 X. W. Xu, J. Q. Liao, H. Jing, and L. M. Kuang, Sci. China-Phys. Mech. Astron. **66**, 100312 (2023), arXiv: 2208.08187.
104 R. Huang, A. Miranowicz, J. Q. Liao, F. Nori, and H. Jing, Phys. Rev. Lett. **121**, 153601 (2018), arXiv: 1807.10084.
105 Y. W. Lu, J. F. Liu, Z. Liao, and X. H. Wang, Sci. China-Phys. Mech. Astron. **64**, 274212 (2021).
106 Y. F. Jiao, S. D. Zhang, Y. L. Zhang, A. Miranowicz, L. M. Kuang, and H. Jing, Phys. Rev. Lett. **125**, 143605 (2020), arXiv: 2002.11148.
107 J. X. Liu, Y. F. Jiao, Y. Li, X. W. Xu, Q. Y. He, and H. Jing, Sci. China-Phys. Mech. Astron. **66**, 230312 (2023), arXiv: 2209.12508.

Appendix

A1 Derivation of the Hamiltonian

We consider a compound COM system of two coupled resonators with the same resonance frequency ω_a. One of the resonators R_1 supports a mechanical breathing mode with frequency ω_m and effective mass m. The second resonator R_2 is a purely optical resonator that is coupled to the first resonator via an evanescent field with a coupling strength of J_0. For simplicity, all directional subscripts are omitted. In the case of forward-input, the total Hamiltonian of this compound COM system can be written as follows ($\hbar = 1$):

$$\begin{aligned} H' = {} & \omega_a a_1^\dagger a_1 + \omega_a a_2^\dagger a_2 + \omega_m b^\dagger b + J_0(a_1^\dagger a_2 + a_2^\dagger a_1) \\ & + \omega_c c^\dagger c + g_d(a_2^{\dagger 2} c + a_2^2 c^\dagger) - g x_0 a_1^\dagger a_1 (b + b^\dagger) \\ & + \mathrm{i}\varepsilon_l(a_1^\dagger \mathrm{e}^{-\mathrm{i}\omega_l t} - a_1 \mathrm{e}^{\mathrm{i}\omega_l t}) + \mathrm{i}\lambda_p(c^\dagger \mathrm{e}^{-\mathrm{i}\omega_p t} - c\mathrm{e}^{\mathrm{i}\omega_p t}), \end{aligned} \tag{a1}$$

where ω_c is the frequency of the second-harmonic modes in R_2. g and g_d are the COM coupling rate in the radiation-pressure process and the nonlinear single-photon coupling strength in the parametric nonlinear process. $\varepsilon_l = \sqrt{2\kappa_1 P_{\mathrm{in}}/\hbar\omega_l}$ is the driving amplitude with input power P_{in}, $\lambda_p = \sqrt{2\kappa_2 P_p/\hbar\omega_p}$ is the pump light with the power P_p, here

κ_1 and κ_2 are the decay rates. By using the unitary transformation $U = \exp\left[\left(-\mathrm{i}\frac{\omega_p}{2}a_1^\dagger a_1 - \mathrm{i}\frac{\omega_p}{2}a_2^\dagger a_2 - \mathrm{i}\omega_p c^\dagger c\right)t\right]$, the Hamiltonian H' can be transformed into the rotating frame, i.e.,

$$H'' = U^\dagger H' U - \mathrm{i}U^\dagger \frac{\partial U}{\partial t}. \tag{a2}$$

Then we have

$$\begin{aligned} H'' = & -\Delta' a_1^\dagger a_1 - \Delta' a_2^\dagger a_2 + \omega_m b^\dagger b + J_0(a_1^\dagger a_2 + a_2^\dagger a_1) \\ & - \Delta_c c^\dagger c + g_d(a_2^{\dagger 2} c + a_2^2 c^\dagger) - g x_0 a_1^\dagger a_1 (b + b^\dagger) \\ & + \mathrm{i}\varepsilon_l(a_1^\dagger \mathrm{e}^{-\mathrm{i}\Delta_{\mathrm{in}} t} - a_1 \mathrm{e}^{\mathrm{i}\Delta_{\mathrm{in}} t}) + \mathrm{i}\lambda_p(c^\dagger - c), \end{aligned} \tag{a3}$$

where $\Delta' = \omega_p/2 - \omega_a$, $\Delta_c = \omega_p - \omega_c$, and $\Delta_{\mathrm{in}} = \omega_l - \omega_p/2$. The dynamical equation of c can be solved by the Heisenberg equation:

$$\dot{c} = \left(\mathrm{i}\Delta_c - \kappa_p\right)c + \lambda_p - \mathrm{i}g_d a_2^2. \tag{a4}$$

Here, we consider the strong pump field to excite mode c in R_2 [65]. Then we get the steady-state solution as:

$$c_s = \frac{-\lambda_p}{\mathrm{i}\Delta_c - \kappa_p}. \tag{a5}$$

After that, the Hamiltonian can be rewritten as follows:

$$\begin{aligned} H'' = & -\Delta' a_1^\dagger a_1 - \Delta' a_2^\dagger a_2 + \omega_m b^\dagger b \\ & + J_0(a_1^\dagger a_2 + a_2^\dagger a_1) - g x_0 a_1^\dagger a_1 (b + b^\dagger) \\ & + \mathrm{i}\varepsilon_l(a_1^\dagger \mathrm{e}^{-\mathrm{i}\Delta_{\mathrm{in}} t} - a_1 \mathrm{e}^{\mathrm{i}\Delta_{\mathrm{in}} t}) + \frac{\Lambda}{2}(a_2^{\dagger 2}\mathrm{e}^{-\mathrm{i}\theta} + a_2^2 \mathrm{e}^{\mathrm{i}\theta}), \end{aligned} \tag{a6}$$

where the strength and the phase are

$$\Lambda = 2g_d\sqrt{\frac{2\kappa_2 P_p}{\left(\Delta_c^2 + \kappa_p^2\right)\hbar\omega_p}}, \quad \theta = -\operatorname{Arg}(c_s). \tag{a7}$$

Due to the resonance condition, we have $\omega_p = \omega_c$. Thus the pump power can be obtained as:

$$P_p = \frac{\hbar\omega_p \kappa_p^2 \Lambda^2}{8 g_d^2 \kappa_2}. \tag{a8}$$

In a frame rotating at frequency Δ_{in}, the total Hamiltonian of this system can be written in the simplest level as follows:

$$\begin{aligned} \mathcal{H} = & -\Delta_l a_1^\dagger a_1 - \Delta_l a_2^\dagger a_2 + \omega_m b^\dagger b \\ & + J_0(a_1^\dagger a_2 + a_2^\dagger a_1) - g x_0 a_1^\dagger a_1 (b + b^\dagger) \\ & + \mathrm{i}\varepsilon_l(a_1^\dagger - a_1) + \frac{\Lambda}{2}(a_2^{\dagger 2}\mathrm{e}^{-\mathrm{i}\theta} + a_2^2 \mathrm{e}^{\mathrm{i}\theta}), \end{aligned} \tag{a9}$$

where $\Delta_l = \Delta_{\mathrm{in}} - \Delta' = \omega_l - \omega_1 = \omega_l - \omega_2$. To diagonalize $\mathcal{H}$, we define the squeezed operator a_s via the Bogoliubov transformation [66-68] $a_s = \cosh(r)a_2 + \mathrm{e}^{-\mathrm{i}\theta}\sinh(r)a_2^\dagger$, with the squeezing parameter $r = (1/4)\ln[(\Delta_l - \Lambda)/(\Delta_l + \Lambda)]$. The Hamiltonian $\mathcal{H}$ becomes

$$\begin{aligned} \mathcal{H} = & -\Delta_l a_1^\dagger a_1 + \omega_m b^\dagger b - g x_0 a_1^\dagger a_1 (b + b^\dagger) \\ & - [\Delta_l(\cosh^2(r) + \sinh^2(r)) + 2\Lambda\cosh(r)\sinh(r)]a_s^\dagger a_s \\ & - \Delta_l \sinh^2(r) - \Lambda\cosh(r)\sinh(r) + \mathrm{i}\varepsilon_l(a_1^\dagger - a_1) \\ & + J_0\cosh(r)(a_1^\dagger a_s + a_s^\dagger a_1) \\ & - J_0\sinh(r)(\mathrm{e}^{-\mathrm{i}\theta}a_1^\dagger a_s^\dagger + \mathrm{e}^{\mathrm{i}\theta}a_1 a_s). \end{aligned} \tag{a10}$$

Then, with the rotating wave approximation and neglecting the constant term [66-68], the Hamiltonian of the system can be written as follows:

$$\begin{aligned} \mathcal{H} = & -\Delta_l a_1^\dagger a_1 - \Delta_s a_s^\dagger a_s + J_s(a_1^\dagger a_s + a_s^\dagger a_1) \\ & + \omega_m b^\dagger b - g x_0 a_1^\dagger a_1 (b + b^\dagger) + \mathrm{i}\varepsilon_l(a_1^\dagger - a_1), \end{aligned} \tag{a11}$$

where $\Delta_s = (\Delta_l + \Lambda)\exp(2r)$, $J_s = J_0\cosh(r)$. This Hamiltonian sets the stage for our calculations of the mechanical gain and the threshold power in the forward-input case. For the backward-input case, we have $J_s = J_0$, and $\Delta_s = \Delta_l$. Then, the Heisenberg equations of motion are written as:

$$\begin{aligned} \dot{a}_1 &= (\mathrm{i}\Delta_l - \kappa_1)a_1 + \mathrm{i}g x_0(b + b^\dagger)a_1 - \mathrm{i}J_s a_s + \varepsilon_l, \\ \dot{a}_s &= (\mathrm{i}\Delta_s - \kappa_2)\, a_s - \mathrm{i}J_s a_1, \\ \dot{b} &= -(\mathrm{i}\omega_m + \gamma_m)\, b - \mathrm{i}g x_0 a_1^\dagger a_1, \end{aligned} \tag{a12}$$

where γ_m is the damping rate of the mechanical mode. As already confirmed in experiments with a COM-based phonon laser [14-16], for a strong driving field, the input noise terms can be safely ignored if one is interested only in the mean-number behaviors (i.e., the threshold feature of the mechanical gain or the phonon amplification). Then, the steady-state solutions can be obtained as:

$$\begin{aligned} \alpha_1 &= \frac{\varepsilon_l(\kappa_2 - \mathrm{i}\Delta_s)}{(\kappa_1 - \mathrm{i}\Delta_l - \mathrm{i}g x_s)(\kappa_2 - \mathrm{i}\Delta_s) + J_s^2}, \\ \alpha_s &= \frac{J_s\alpha_1}{\Delta_s + \mathrm{i}\kappa_2}, \quad \beta = \frac{g x_s |\alpha_1|^2}{\omega_m - \mathrm{i}\gamma_m}, \end{aligned} \tag{a13}$$

where $x_s = x_0(\beta + \beta^*)$ is the steady-state mechanical displacement.

A2 Derivation of the mechanical gain

We introduce the supermode operators $a_\pm = (a_1 \pm a_s)/\sqrt{2}$, which satisfy the commutation relations $[a_+, a_+^\dagger] = [a_-, a_-^\dagger] = 1$, $[a_+, a_-^\dagger] = 0$. Eq. (a11) can be written as:

$$\begin{aligned} H = & \omega_+ a_+^\dagger a_+ + \omega_- a_-^\dagger a_- + \omega_m b^\dagger b, \\ & - \frac{g x_0}{2}[(a_+^\dagger a_+ + a_-^\dagger a_-) + (a_+^\dagger a_- + a_-^\dagger a_+)](b^\dagger + b) \\ & + \frac{\Delta}{2}(a_+^\dagger a_- + a_-^\dagger a_+) + \frac{\mathrm{i}\varepsilon_l}{\sqrt{2}}[(a_+^\dagger + a_-^\dagger) - (a_+ + a_-)], \end{aligned} \tag{a14}$$

with the supermode frequencies $\omega_\pm = -(\Delta_s + \Delta_l)/2 \pm J_s$, and $\Delta = \Delta_s - \Delta_l$. Under the rotating-wave approximation condition $2J_s + \omega_m,\ \omega_m \gg |2J_s - \omega_m|$ [63,64]. Thus we have

$$\begin{aligned} H =& \omega_+ a_+^\dagger a_+ + \omega_- a_-^\dagger a_- + \frac{\Delta}{2}(a_+^\dagger a_- + a_-^\dagger a_+) \\ &+ \omega_m b^\dagger b - \frac{g x_0}{2}(a_+^\dagger a_- b + b^\dagger a_-^\dagger a_+) \\ &+ \frac{\mathrm{i}\varepsilon_l}{\sqrt{2}}[(a_+^\dagger + a_-^\dagger) - (a_+ + a_-)]. \end{aligned} \tag{a15}$$

In the supermode picture, the dynamical equations of the system can be written as:

$$\begin{aligned} \dot{a}_+ &= -(\mathrm{i}\omega_+ + \kappa_0)a_+ + \frac{\mathrm{i}}{2}(g x_0 b - \Delta)a_- + \frac{\varepsilon_l}{\sqrt{2}}, \\ \dot{a}_- &= -(\mathrm{i}\omega_- + \kappa_0)a_- + \frac{\mathrm{i}}{2}(g x_0 b^\dagger - \Delta)a_+ + \frac{\varepsilon_l}{\sqrt{2}}, \\ \dot{b} &= -(\mathrm{i}\omega_m + \gamma_m)b + \frac{\mathrm{i}g x_0}{2} a_+ a_-^\dagger, \end{aligned} \tag{a16}$$

where $\kappa_0 = (\kappa_1 + \kappa_2)/2$. With the ladder operator $p = a_-^\dagger a_+$ and population inversion operator $\delta n = a_+^\dagger a_+ - a_-^\dagger a_-$, the dynamical equations of the system are then read

$$\dot{b} = -(\gamma_m + \mathrm{i}\omega_m)b + \frac{\mathrm{i}g x_0}{2} p, \tag{a17}$$

$$\dot{p} = -2(\kappa_0 + \mathrm{i}J_s)p + \frac{\mathrm{i}}{2}(\Delta - g x_0 b)\delta n + \frac{\varepsilon_l}{\sqrt{2}}(a_+ + a_-^\dagger). \tag{a18}$$

By setting the time derivatives of $a_\pm$ and p as zero, we can solve the steady-state solutions of the system, i.e.,

$$\begin{aligned} p &= \frac{\sqrt{2}\varepsilon_l(a_+ + a_-^\dagger) - \mathrm{i}(g x_0 b - \Delta)\delta n}{2\mathrm{i}(2J_s - \omega_m) + 4\kappa_0}, \\ a_+ &= \frac{\varepsilon_l(2\mathrm{i}\omega_- + 2\kappa_0 + \mathrm{i}g x_0 b - \mathrm{i}\Delta)}{2\sqrt{2}[D - \mathrm{i}(\Delta_l + \Delta_s)\kappa_0]}, \\ a_- &= \frac{\varepsilon_l(2\mathrm{i}\omega_+ + 2\kappa_0 + \mathrm{i}g x_0 b^\dagger - \mathrm{i}\Delta)}{2\sqrt{2}[D - \mathrm{i}(\Delta_l + \Delta_s)\kappa_0]}, \end{aligned} \tag{a19}$$

with

$$D = J_s^2 + \kappa_0^2 - \Delta_s\Delta_l + \frac{[g^2 x_0^2 n_b - 2g x_0 \Delta \mathrm{Re}(b)]}{4},$$

where $n_b = b^\dagger b$. Substituting eq. (a19) into the dynamical equation of b in eq. (a17) results in

$$\dot{b} = (-\mathrm{i}\omega_m - \mathrm{i}\omega' + G - \gamma_m)b + F, \tag{a20}$$

where

$$\begin{aligned} \omega' =& \frac{g^2 x_0^2 (2J_s - \omega_m)\delta n}{4(2J_s - \omega_m)^2 + 16\kappa_0^2} \\ &+ \frac{g^2 x_0^2 \varepsilon_l^2 \kappa_0^2 (\Delta_l + \Delta_s)}{[2(2J_s - \omega_m)^2 + 8\kappa_0^2][D^2 + (\Delta_l + \Delta_s)^2\kappa_0^2]}, \\ F =& \frac{g x_0 \Delta \delta n}{4\mathrm{i}(2J_s - \omega_m) + 8\kappa_0} \\ &+ \frac{\mathrm{i}g x_0 \varepsilon_l^2 [D(\kappa_0 - \mathrm{i}J_s) + \kappa_0(\Delta_l + \Delta_s)\Delta_s]}{[2\mathrm{i}(2J_s - \omega_m) + 4\kappa_0][D^2 + (\Delta_l + \Delta_s)^2\kappa_0^2]}, \end{aligned}$$

and the mechanical gain is

$$\begin{aligned} G =& G_0 + \mathcal{G} \\ =& \frac{g^2 x_0^2 \kappa_0 \delta n}{2(2J_s - \omega_m)^2 + 8\kappa_0^2} \\ &+ \frac{\varepsilon_l^2 g^2 x_0^2 (\omega_m - 2J_s)(\Delta_s + \Delta_l)\kappa_0}{\left[4(2J_s - \omega_m)^2 + 16\kappa_0^2\right]\left[D^2 + (\Delta_l + \Delta_s)^2\kappa_0^2\right]}, \end{aligned} \tag{a21}$$

with

$$\delta n = \frac{\varepsilon_l^2\,[2J_s\Delta_s - \kappa_0 g x_0 \mathrm{Im}(b) - J_s g x_0 \mathrm{Re}(b)]}{D^2 + \kappa_0^2(\Delta_l + \Delta_s)^2}.$$